

## Tetrathiomolybdate Inhibits Copper Trafficking Proteins Through Metal Cluster Formation

Hamsell M. Alvarez,<sup>1\*</sup> Yi Xue,<sup>1\*</sup> Chandler D. Robinson,<sup>1</sup> Mónica A. Canalizo-Hernández,<sup>1</sup> Rebecca G. Marvin,<sup>1</sup> Rebekah A. Kelly,<sup>3</sup> Alfonso Mondragón,<sup>2</sup> James E. Penner-Hahn,<sup>3</sup> Thomas V. O'Halloran<sup>1,2,†</sup>

<sup>1</sup>The Chemistry of Life Processes Institute, Northwestern University, Evanston, IL 60208, USA. <sup>2</sup>Department of Biochemistry, Molecular Biology and Cell Biology, Northwestern University, Evanston, IL 60208, USA. <sup>3</sup>Department of Chemistry, The University of Michigan, Ann Arbor, MI 48109, USA.

\*These authors contributed equally to this work.

†To whom correspondence should be addressed. E-mail: t-ohalloran@northwestern.edu

**Tetrathiomolybdate (TM) is an orally active agent for treatment of disorders of copper metabolism. Here we describe how TM inhibits proteins that regulate copper physiology. Crystallographic results reveal that the surprising stability of the drug complex with the metallochaperone Atx1 arises from formation of a sulfur-bridged copper-molybdenum cluster reminiscent of those found in molybdenum and iron sulfur proteins. Spectroscopic studies indicate that this cluster is stable in solution and corresponds to physiological clusters isolated from TM-treated Wilson's disease animal models. Finally, mechanistic studies show that the drug-metallochaperone inhibits metal transfer functions between copper trafficking proteins. The results are consistent with a model wherein TM can directly and reversibly down-regulate copper delivery to secreted metalloenzymes and suggest that proteins involved in metal regulation might be fruitful drug targets.**

Excess dietary molybdate ( $\text{MoO}_4^{2-}$ ) uptake was first linked to a fatal disorder in cattle known as 'teart' pastures syndrome (1) and later to a neurological disorder in sheep known as 'Swayback' (2). Both disorders arise from Mo-induced copper deficiency and the symptoms are readily reversed with copper supplementation. While molybdate itself has little or no affinity for copper ions, the active copper-depleting agent, TM ( $\text{MoS}_4^{2-}$ ), is formed in the ruminants digestive track and readily reacts with  $\text{Cu}^I$  or  $\text{Cu}^{II}$  to form insoluble compounds. These zoogenic studies inspired the development of molybdenum compounds to treat copper-dependent diseases in humans (3). The potent chelating and antiangiogenic activities of orally-active formulation of TM, such as the ammonium salt  $[(\text{NH}_4)_2(\text{MoS}_4)]$  (4-6) and the choline salt (ATN-224) (7,8) have been used in treatment of Wilson disease, where copper accumulation leads to hepatic and neurological disorders; as well as in the inhibition of metastatic cancer progression in a number of clinical trials (9-

11). TM inhibits several copper enzymes including ceruloplasmin (Cp), ascorbate oxidase, cytochrome oxidase, superoxide dismutase (SOD1), tyrosinase, and the *Enterococcus hirae* ATPase (CopB) (12,13), and also downregulates the expression of cytokines such as the vascular endothelial growth factor (VEGF), as well as transcription factors such as the nuclear factor- $\kappa\text{B}$  (NF- $\kappa\text{B}$ ), involved in angiogenesis signaling pathways (14,15). While TM can bind to Cu-Cp (12), copper serum albumin (Cu-BSA) (16) and Cu-containing metallothioneins (Cu-MT) (17), and has been proposed to inhibit SOD1 by partially removing copper from the enzyme (8,18) the reaction chemistry and structures of these complexes have not been resolved.

Metallochaperones constitute a particular kind of protein that delivers metal ions to specific cytoplasmic targets in the cell (19). The prototypical metallochaperone, yeast Atx1, transfers  $\text{Cu}^I$  along a trafficking pathway via electrostatic interactions with structurally-homologous N-terminal domains of the ATPase, Ccc2 (20,21). Likewise, the closely related human copper metallochaperone, Atox1 can transfer copper to N-terminal domains of the copper-transporting ATPases 7a and 7b, also known as the Menkes and Wilson disease proteins. All three of these proteins are important in mammalian copper homeostasis and provide copper to secreted enzymes that are important in vascular integrity such as Cp and extracellular SOD (ecSOD). We anticipated that TM would readily remove  $\text{Cu}^I$  from its binding site in Atx1 with subsequent formation of a typical polymeric  $\text{CuMo}$  sulfide precipitate. We found instead a robust TM-metallochaperone complex with metal sulfur ratios reminiscent of the FeMo cofactor-complex in nitrogenase (22) and elucidated how this antiangiogenic drug affects the structure and function of this canonical metal trafficking domain.

Direct reaction of TM with Cu-Atx1 leads to rapid formation of an air stable purple complex that can be readily

isolated by size exclusion chromatography (23). Crystals of this complex diffract to 2.3 Å (fig. S1) and the X-ray structure reveals the presence of 12 Cu-Atx1 molecules in the asymmetric unit arranged as four TM-Cu-Atx1 non-crystallographic trimers (fig. S2). The overall structure of each Atx1 monomer is similar to previously determined structures, retaining the ‘ferredoxin-like’  $\beta\alpha\beta\beta\alpha\beta$  fold (24), with two cysteines involved in copper binding (Cys15 and Cys18) located at the protein surface. Superposition of the coordinates of Hg-Atx1 (PDB code 1CC8) (24) and Cu-Atox1 (human analog of Atx1, PDB code 1FEE) (25) on the monomers in the complex (Fig. 1C and 1D) reveals that the peptide fold around the metal binding loop is unperturbed by TM binding, with an average rms deviation for the  $C_\alpha$  atoms of  $\sim 0.67$  Å (Hg-Atx1) and  $\sim 1.3$  Å (Cu-Atox1). In the structure, each Atx1 trimer coordinates four copper atoms and one TM molecule, with the stoichiometry  $[\text{TM}][(\text{Cu})(\text{Cu-Atx1})_3]$ , which is corroborated by independent elemental analysis of the complex (23). The Cu x-ray absorption near-edge structure of the complex indicates that the copper remains in the  $\text{Cu}^{\text{I}}$  oxidation state, while the Mo K near-edge spectrum strongly resembles that of tetrathiomolybdate ( $\text{Mo}^{\text{VI}}$ ) (fig. S3). Aside from a few H-bonding interactions between monomers, the dominant forces stabilizing the trimer are the coordinate covalent bonds between the protein CysS atoms and the metal cluster.

A ‘nest-shaped’ copper-molybdenum cluster, unprecedented in metalloproteins, is located at the center of the Atx1 trimer (Fig. 1A and 1B) on the three-fold axis. The cluster consists of four  $\text{Cu}^{\text{I}}$  ions,  $[\text{MoS}_4]^{2-}$  and three pairs of Atx1 CysS atoms to give a  $[\text{S}_6\text{Cu}_4\text{MoS}_4]$  cluster (Fig. 2). The Mo atom remains tetrahedrally coordinated by four sulfide ions with Mo-S distances in the range 2.18 - 2.26 Å (mean: 2.22 Å), as expected for Cu-S-Mo cluster interactions and commensurate with the ones observed in the parent drug (2.17 - 2.20 Å, mean: 2.19 Å) (7). Three of the copper atoms bind to the sulfur atoms of cysteines 15 and 18, and each of these atoms also binds two sulfides from  $[\text{MoS}_4]^{2-}$  resulting in a distorted tetrahedral coordination environment for the coppers with similar distances for the Cu-S bonds to protein sidechains (2.21 - 2.44 Å, mean: 2.30 Å) or the sulfides of TM (2.24 - 2.40 Å, mean: 2.29 Å). The Mo-Cu distances are in the range of 2.74 - 2.82 Å (mean: 2.77 Å). The fourth sulfide of TM does not coordinate copper or interact with protein. On the other side of the complex, the fourth copper atom is bound by three (Cys15) $\text{S}_\gamma$  atoms (2.22 - 2.30 Å, mean: 2.26 Å) and exhibits a trigonal planar coordination. Thus, three of the four sulfide ions in TM form a  $\mu_3$ -S bridge between the Mo atom and two tetrahedral Cu atoms, whereas each of the (Cys15) $\text{S}_\gamma$  atoms of three Atx1 behave as a bridging ligand between one tetrahedral and one trigonal planar copper center. In the tetrahedrally coordinated coppers,

the (Cys15) $\text{S}_\gamma$ -Cu-S $\gamma$ (Cys18) bond angles are larger (118 - 125°, mean: 122°) than the (TM)S-Cu-S(TM) bond angles (99-103°, mean: 101°), consistent with a distorted tetrahedral site. The geometry at the Mo atom is only slightly distorted from tetrahedral, with (TM)( $\mu_3$ -S)-Mo-( $\mu_3$ -S)(TM) and (TM)( $\mu_3$ -S)-Mo-S(TM) bond angles of 103 - 110° (mean: 106°) and 109 - 116° (mean: 112°), respectively. Protein-TM interactions partially neutralize the negative charge delocalized over the  $[\text{Cu}_4\text{MoS}_4]^+$  cluster (fig. S4 and Fig. 2A). Three positively charged lysines (Lys65) form hydrogen bonds with the sulfides from TM and the thiolates of Cys18. Strong interactions are observed for the only terminal S thiolate ligands in the cluster (Cys18-S-Lys65-N $\zeta$  = 3.3 Å) relative to  $\mu_3$ -S bridging sulfide ligands (TM- $\mu_3$ -S-Lys65-N $\zeta$  = 3.8 Å). In addition, H-bonds from backbone amides (Thr14 and Gly17) at the amino-terminus of  $\alpha$  helix 2 to metal-bound thiolates further neutralize the negative charge of the buried cluster.

While this type of cluster has not been previously reported in metalloproteins, analogous ‘nest-shaped’  $[\text{Cu}_3\text{MoS}_3\text{O}]$  inorganic units (with P- and N-donor ligands) are components of larger clusters (26). The closest fragment analog of the protein-drug adduct is a component of the  $[\text{Bu}^n\text{N}]_4[\text{Cu}_{12}\text{Mo}_8\text{S}_{32}]$  complex: here, a  $[\text{S}_6\text{Cu}_3\text{MoS}_4]$  unit, exhibits similar bond distances (Mo-Cu = 2.69 ~ 2.75 Å, Mo-S = 2.06 ~ 2.25 Å and Cu-S = 2.29 ~ 2.36 Å) (27) and geometry (fig. S5). Another structurally distinct CuSMo center is observed in the Cu-Mo-pterin enzyme carbon monoxide dehydrogenase from *Oligotropha carboxidovorans*, where a single diagonally coordinated Cu atom is bound via a bridging sulfide to a Mo active site forming a  $[\text{CuSMo}(=\text{O})\text{OH}]$  cluster (28).

In order to determine whether TM interaction with Atx1 inhibits its copper chaperone activity, we developed a native gel based copper transfer assay which monitors metal occupancy in a mixture of TM-Cu-Atx1 trimer and Ccc2a, the physiological partner of Atx1 (fig. S6). The assay takes advantage of the fact that apo- and Cu-Atx1 are clearly distinguishable from Ccc2a and TM-Cu-Atx1 in a native agarose gel system (23), where the protein and metal content of the bands are characterized by a variety of analytical techniques to establish the metallation state of each protein (fig. S7 to S12 and table S1). The assay was validated by a combination of protein mass spectrometry (ESI-MS) and, quantitative elemental analysis (ICP-MS) of samples extracted from gel slices, as well as by qualitative laser scanning elemental analysis (LA-ICP-MS) of the electrophoresis gel itself. Three key lanes are shown in Fig. 3A. The TM-Cu-Atx1(SeMet) migrates as a positive species containing copper and molybdenum (Lane I). Mixing of apo-Ccc2a and Cu-Atx1(SeMet) results in the transfer of copper from Cu-Atx1(SeMet) to Ccc2a (Lane II). The transfer of

copper from Atx1(SeMet) to Ccc2a is almost completely abolished by the presence of TM (lane III). Both native Atx1 and the SeMet analog give similar results. Intriguingly, protein analysis indicates formation of a new Cu-TM protein complex, which contains the Ccc2 domain as well as TM and Cu-Atx1. The formation of this heteromeric protein complex suggests that other proteins with surface-exposed MxCxxC copper binding motif will be able to form similar complexes with TM.

These results suggest a new model for how a drug can disrupt a key protein-protein interaction for metal trafficking pathways. Support for the physiological occurrence of this type of metal-protein cluster is shown in Fig. 3B by the highly similar Cu and Mo K-edge extended x-ray absorption fine structure analysis of the [TM]([Cu)(Cu-Atx1)<sub>3</sub>] complex, and a kidney sample extracted from TM-treated LPP rats (animal model of Wilson's disease), where a similar [(CuSR)<sub>3</sub>S<sub>4</sub>Mo]<sup>2-</sup> type interaction is proposed (29). The stoichiometry of three chaperone molecules and four copper atoms per drug molecule has several physiological implications. By sequestering multiple copper chaperones and the metal cargo destined for trafficking to the trans-Golgi, TM may suppress Cu incorporation into secreted copper enzymes including those involved in modification of the vasculature such as ecSOD, copper amine oxidases, lysyl oxidase, and Cp. The TM-mediated sequestration of copper loaded metallochaperones may perturb other proposed roles of Atox1 in regulation of copper-related tumor angiogenic factors (30).

The structure and biochemistry of the TM-Cu-Atx1 complex also provides chemical insights into the puzzling stoichiometry of the Cu-Mo antagonism (31), and suggests why ternary complex formation between TM and specific Cu-proteins can have pronounced physiological consequences (32). A relatively small amount of dietary molybdenum clearly perturbs the timely dissemination of a larger pool of copper in deficiency disorders such as 'swayback' and 'teart' pasture syndrome. Our results raise the possibility that the active agent, TM, functionally suppresses copper trafficking domains that control the secretion of the active forms of copper-dependent enzymes. Finally, our results suggest that proteins involved in such metallation pathways may be targets for the development of new classes of pharmaceutical agents.

## References and Notes

1. W. S. Ferguson, A. H. Lewis, S. J. Watson. *Nature* **141**, 553 (1938).
2. C. F. Mills, B. F. Fell, *Nature* **185**, 20 (1960).
3. Brewer, G. J. *Exp. Biol. Med.* **226**, 665 (2001).
4. J. M. Walshe, in *Orphan Diseases and Orphan Drugs*, I. H. Scheinberg, J. M. Walshe, Eds. (Manchester Univ. Press, Manchester, UK, 1986), pp. 76–85.
5. G. J. Brewer *et al.*, *Arch. Neurol.* **48**, 42 (1991).
6. P. J. Sadler, C. Muncie, M. A. Shipman, in *Biological Inorganic Chemistry, Structure and Reactivity*, I. Bertini, H. B. Gray, E. I. Stiefel, J. S. Valentine, Eds. (University Science Books, Sausalito, CA, 2007), pp. 95–135.
7. V. E. Lee, J. M. Schulman, E. I. Stiefel, C. C. Lee, *J. Inorg. Biochem.* **101**, 1707 (2007).
8. J. C. Juarez *et al.*, *Clin. Cancer Res.* **12**, 4974 (2006).
9. G. J. Brewer *et al.*, *Clin. Cancer Res.* **6**, 1 (2000).
10. B. G. Redman *et al.*, *Clin. Cancer Res.* **9**, 1666 (2003).
11. ClinicalTrials.gov, Page. Active trials: TM (2001), ATN-224 (2006).
12. M. V. Chidambaram, G. Barnes, E. Frieden, *J. Inorg. Biochem.* **22**, 231 (1984).
13. K. D. Bissig, T. C. Voegelin, M. Solioz, *FEBS Lett* **507**, 367 (2001).
14. L. Mandinov *et al.*, *Proc. Natl. Acad. Sci. U.S.A.* **100**, 6700 (2003).
15. Q. Pan *et al.*, *Cancer Res.* **62**, 4854 (2002).
16. E. K. Quagraine, R. S. Reid, *J. Inorg. Biochem.* **85**, 53 (2001).
17. K. T. Suzuki, Y. Ogra, *Res. Commun. Mol. Pathol. Pharmacol.* **88**, 187 (1995).
18. J. C. Juarez *et al.*, *Proc. Natl. Acad. Sci., USA* **105**, 7147 (2008).
19. L. A. Finney, T. V. O'Halloran, *Science* **300**, 931 (2003).
20. R. A. Pufahl *et al.*, *Science* **278**, 853 (1997).
21. D. L. Huffman, T. V. O'Halloran, *J. Biol. Chem.* **275**, 18611 (2000).
22. J. B. Howard, D. C. Rees, *Proc. Natl. Acad. Sci. U.S.A.* **103**, 17088 (2006).
23. Material and methods are available as supporting material on Science Online.
24. A. C. Rosenzweig *et al.*, *Structure* **7**, 605 (1999).
25. A. K. Wernimont, D. L. Huffman, A. L. Lamb, T. V. O'Halloran, A. C. Rosenzweig, *Nat. Struct. Biol.* **7**, 766 (2000).
26. C. Zhang *et al.*, *Eur. J. Inorg. Chem.*, 55 (2002).
27. J. G. Li, X. Q. Xin, Z. Y. Zhou, *J. Chem. Soc., Chem. Commun.*, 249 (1991).
28. H. Dobbek, L. Gremer, R. Kiefersauer, R. Huber, O. Meyer, *Proc. Natl. Acad. Sci. U.S.A.* **99**, 15971 (2002).
29. L. Zhang *et al.*, *Biochemistry* **48**, 891 (2009).
30. S. Itoh *et al.*, *J. Biol. Chem.* **283**, 9157 (2008).
31. H. R. Marston, *Physiol. Rev.* **32**, 66 (1952).
32. C. F. Mills, *Philos. Trans. R. Soc. Lond. Ser. B.* **288**, 51 (1979).
33. This manuscript is dedicated to the memory of Prof. E. Stiefel and his contributions to the field of molybdenum sulfide chemistry. This work was supported by grants GM54222 and GM38784 (T.V.O.) and GM38047 (J.E.P.-H.) from the NIH. The Robert H. Lurie Comprehensive

Cancer Center provided a Malkin Fellowship (H.M.A.) and support for Structural Biology Facility. Use of the Advanced Photon Source (SBC-CAT and IMCA-CAT) and the Stanford Synchrotron Radiation Laboratory was supported by the U. S. Department of Energy, Office of Basic Energy Sciences, with additional support (at SSRL) from NIH-NCRR. Use of the CBC-UIC Proteomics Facility was supported by The Searle Funds at the Chicago Biomedical Consortium, and use of LA-ICP-MS was supported by a NASA grant to the Quantitative Bioelement Imaging Center in the Chemistry of Life Processes Institute at Northwestern University. We thank P. Focia for assistance with X-ray diffraction collection, M. Clausén for assistance in the early stages of XAS measurements, Y. Wang for assistance with the protein MS, A. Davis for providing *apo-Ccc2a*, and A. Mazar for helpful discussions. The atomic coordinates have been deposited at the Protein Data Bank with code 3K7R.

### Supporting Online Material

[www.sciencemag.org/cgi/content/full/1179907/DC1](http://www.sciencemag.org/cgi/content/full/1179907/DC1)

Materials and Methods

Fig. S1 to S16

Table S1 to S4

References

Movie S1

30 July 2009; accepted 4 November 2009

Published online 26 November 2009;

10.1126/science.1179907

Include this information when citing this paper

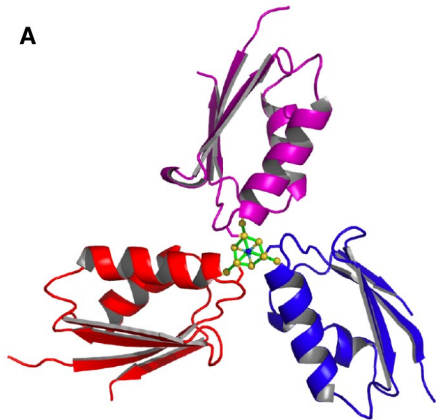
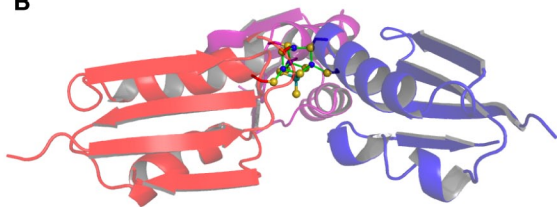
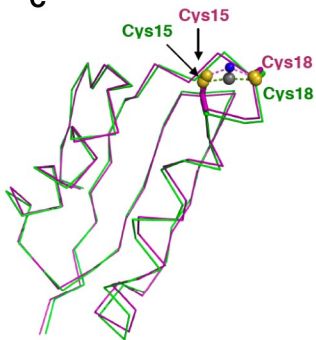
**Fig. 1.** Structure of the [TM]((Cu)(Cu-Atx1)<sub>3</sub>) drug-protein adduct and comparison of Hg-Atx1 and Cu-Atox1 with Cu-Atx1 (monomer B) from the [TM]((Cu)(Cu-Atx1)<sub>3</sub>) complex (see movie S1). (A) Top view of the trimer cluster. (B) Side view of the trimer cluster. Atx1 monomers are shown as blue, purple and red cartoon ribbon diagrams, and copper atoms are shown as blue spheres. The TM and metal binding cysteines are represented with a ball-and-stick model, where a molybdenum atom is shown as a cyan sphere, and sulfur atoms are shown as yellow spheres. The coordination bonds are denoted with green dashed lines. Superposition of Cu-Atx1 (monomer B) (purple chain) from the TM-Cu-Atx1 complex with (C) Hg-Atx1 (green chain, PDB code 1CC8), and (D) with Cu-Atox1 (cyan chain, PDB code 1FEE). Sulfur atoms from Cys15 (Atx1) and Cys18 (Atx1) are shown as yellow spheres, copper atoms from Cu-Atx1 (monomer B) are shown as blue spheres, mercury atom from Hg-Atx1 is shown as a grey sphere, and copper atom from Cu-Atox1 is shown as a light blue sphere (note: TM is not shown). The similarities of the peptide fold around the metal binding loop regions in these three structures suggest that binding of Cu by

Atx1 in the TM-Cu-Atx1 complex is not disturbed by TM. The Cu coordination environment in Cu-Atx1 from TM-Cu-Atx1 is very similar to the one found in Cu-Atox1 (dimer) (25), but differs with the nearly linear coordination of Hg in Hg-Atx1 (24).

**Fig. 2.** Structure of the ‘nest-shaped’ [S<sub>6</sub>Cu<sub>4</sub>MoS<sub>4</sub>] cluster in the [TM]((Cu)(Cu-Atx1)<sub>3</sub>) trimer complex (see movie S1). (A) Structure of the [S<sub>6</sub>Cu<sub>4</sub>MoS<sub>4</sub>] cluster with average interatomic distances. The cluster is represented with a ball-and-stick model. Atx1 monomers are shown as blue, purple and red cartoon ribbon diagrams. Copper atoms are shown as blue spheres, sulfur atoms from Cys15 (Atx1), Cys18 (Atx1) and TM are shown as yellow spheres, a molybdenum atom is shown as a cyan sphere, and nitrogen atoms from Lys65 (Atx1) are shown as tan spheres. The hydrogen bonds are denoted with yellow dashed lines. (B) Cu anomalous peaks in the final model of the [S<sub>6</sub>Cu<sub>4</sub>MoS<sub>4</sub>] cluster (blue mesh of the anomalous difference Fourier map are contoured at 10.0σ level). Sulfur atoms from Cys15 and Cys18 of each of the three Atx1 are connected by a blue, purple and red lines. The molybdenum atom is tetrahedrally coordinated by four sulfur atoms. The top copper atom displays a trigonal-planar geometry coordinated by thiolates from Cys15 (Atx1), while each of the other three neighboring copper atoms adopts a distorted tetrahedral coordination with ligands from both TM and Atx1.

**Fig. 3.** TM inhibition of Atx1 copper chaperone activity, and physiological relevance of the [TM]((Cu)(Cu-Atx1)<sub>3</sub>) complex. (A) TM interferes with copper transfer from the Atx1(SeMet) copper chaperone to its target Ccc2a. Inhibition of the copper transfer function was assayed by native gel electrophoresis and qualitative LA-ICP-MS. Gel lanes (I, II, and III) were cut from gel (fig. S6). The [TM]((Cu)(Cu-Atx1(SeMet))<sub>3</sub>) (lane I) is represented by band 1, the Cu-Atx1(SeMet) + *apo-Ccc2a* (1:1) mixture (lane II) yields bands 2, 3 and 4, and the [TM]((Cu)(Cu-Atx1(SeMet))<sub>3</sub>) + *apo-Ccc2a* (1:1) mixture (lane III) yields bands 5, 6, 7 and 8. LA-ICP-MS scans are represented by the intensities (CPS: counts per second) of <sup>65</sup>Cu (blue) and <sup>95</sup>Mo (pink) (x-axis), and the length of the gel (mm) (y-axis). The protein band lengths are shown as black double-headed arrows (↔), while the protein loading wells are shown as red double-headed arrows (↔). Excision and gel digestion ICP-MS analysis of band 1 shows a Cu/Mo ratio of 3.6 ± 0.09 (table S1), while LA-ICP-MS scans reveal a significant concentration of both metals, leading us to assign band 1 as [TM]((Cu)(Cu-Atx1(SeMet))<sub>3</sub>). Bands 3 (lane II) and 6 (lane III) are identified as the [Atx1(SeMet)-Cu-Ccc2a] heterodimer complex based on metal and protein analysis of each band. Band 7 contains a mixture of apo-Atx1(SeMet) and apo-Ccc2a with an approximate Cu/Mo ratio of 3.1 ± 0.08 (ICP-

MS) (table S1), which is confirmed by a qualitative LA-ICP-MS identification of both metals, indicating the formation of a [(TM)(Cu)(Atx1(SeMet))(Ccc2a)] complex. Elemental analysis by ICP-MS of band 8 reveals copper is at or below the detection limit, indicating that less than 10% of Cu in the TM-Cu-Atx1 complex is transferred to Ccc2a (table S1). Quantitative analysis of the gel slice is consistent with LA-ICP-MS scans showing that most of the Cu of lane III is contained in band 7. These experiments indicate that the formation of the [TM][(Cu)(Cu-Atx1(SeMet))<sub>3</sub>] complex disrupts copper translocation from Cu-Atx1(SeMet) to the domain A of the P-type ATPase Ccc2. **(B)** Cu and Mo K-edge extended x-ray absorption fine structure (EXAFS) Fourier transforms phase shift overlay (experimental data) for [TM][(Cu)(Cu-Atx1)<sub>3</sub>], and a kidney sample extracted from LPP rats treated with TM (from Ref. 29). The slightly higher amplitude of the Mo...Cu peak for the kidney sample compared to the [TM][(Cu)(Cu-Atx1)<sub>3</sub>] reflects the slight difference in the Mo EXAFS best fits, 3 and 2–3 Mo...Cu, respectively. The Cu...Mo peak is slightly more intense for the [TM][(Cu)(Cu-Atx1)<sub>3</sub>] complex than for the kidney sample, modeled by 1 Cu...Mo instead of 0.5, respectively. Cu and Mo K-edge EXAFS spectra and EXAFS Fourier transform including experimental data and best fits are included in figure S13. The fit results are summarized in table S2.

**A****B****C****D**